Chemical Engineering Journal 163 (2010) 126–132

Contents lists available at ScienceDirect

Chemical Engineering Journal

journal homepage: www.elsevier.com/locate/cej

# Flow pattern and break-up of liquid film in single-channel falling film microreactors

Haocui Zhang [a,b], Jun Yue [a], Guangwe Chen [a,*], Quan Yuan [a]

[a] Dalian National Laboratory for Clean Energy, Dalian Institute of Chemical Physics, Chinese Academy of Sciences, Dalian 116023, China
[b] Graduate University, Chinese Academy of Sciences, Beijing 100049, China

ARTICLE INFO

*Article history:*
Received 1 April 2010
Received in revised form 16 July 2010
Accepted 21 July 2010

*Keywords:*
Microchannel
Microreactor
Microfluidics
Falling film
Flow pattern
Minimum wetting flow rate

ABSTRACT

This paper concerns an experimental investigation into the flow pattern transition and break-up mechanism of liquid film in single-channel falling film microreactors. Three major flow patterns were observed to be 'corner rivulet flow', 'falling film flow with dry patches', and 'complete falling film flow'. The critical flow rate associated with the transition between each flow pattern was determined. Hysteresis was found, as the critical flow rate was higher when the flow pattern shifted from 'falling film flow with dry patches' to 'complete falling film flow' than it was when the flow pattern shifted in the opposite direction. There existed a minimum wetting flow rate (MWF) in order to the complete falling film flow pattern to be present. MWF was observed to increase with the width or depth of microchannel and could not be well predicted by traditional falling film correlations. Based on the obtained data, an empirical correlation has been proposed for the prediction of MWF in falling film microreactors, where the influence of fluid physical properties and channel dimension is revealed.



## 1. Introduction

Falling film microreactors have potential applications for chemical processes due to high mass and heat transfer efficiency in a very thin liquid film. For example, falling film microreactors have been demonstrated to benefit a variety of gas–liquid operations including direct fluorination [1], catalytic hydrogenation [2], photochemical chlorination [3], and ozonolysis reaction [4]. It is well known that the completeness and fluctuation characteristics of the liquid film will have a significant influence on its heat and mass transfer performance [5–7]. To further improve the transfer rate and conversion of reactant in the liquid film, one possible way is to reduce the film thickness by decreasing the liquid flow rate. However, the complete falling film in the microchannel will breakup if the film thickness is sufficiently thin, which is obviously disadvantageous to the heat and mass transfer process [8]. To improve the reaction efficiency and optimize the operational condition, it is thus necessary to investigate liquid film break-up mechanism in microchannels.

Flow patterns in falling film microreactors have been shown to be somewhat different from their macroscale counterparts. In a traditional large-sized falling film reactor, the flow pattern usually displays as finger flow, or falling film with dry patches [9]. But due to the micron-sized geometry, the flow pattern in falling film microreactors turns to be corner rivulet flow, falling film flow with dry patches, and complete falling film flow [8]. The complete falling film flow is the most favorable flow pattern for chemical reaction, which is only present when liquid flow rate is kept above a certain rate (defined as the minimum wetting flow rate, MWF). In traditional falling film reactors, there are two available criterions to predict MWF, as suggested by Hartely and Murgatroyd [10]. The first one is the force balance criterion, which is that the surface tension force balances the fluid pressure on the top point of a stable dry patch, and then MWF and the minimum liquid film thickness can be obtained according to the Nusselt falling film velocity distribution. The second one is the minimum total energy criterion stated as the film will breakup if the total energy in a given streamwise length of a liquid rivulet is minimum. Based on these two criteria, some researchers have proposed their empirical correlations (cf. Table 1). Nevertheless, the validity of these correlations in falling film microreactors still remains unclear. This work presents an experimental observation of the flow pattern and break-up mechanism of the liquid film in a set of single-channel falling film microreactors (SFFMR) by using a high-speed CCD camera. The minimum wetting flow rate in microchannels was measured and compared with the prediction of the traditional falling film correlations. It has been found that MWF tended to increase with the width or depth of microchannel and could not be well predicted by the existing correlations. Therefore, new empirical correlations have been proposed for the prediction of MWF in falling film microreactors based on the exper-

* Corresponding author. Tel.: +86 411 84379031; fax: +86 411 84379327.
*E-mail address:* gwchen@dicp.ac.cn (G. Chen).

1385-8947/$ – see front matter © 2010 Elsevier B.V. All rights reserved.
doi:10.1016/j.cej.2010.07.045

## Nomenclature

*Nomenclature*

| | |
|---|---|
| $g$ | gravity acceleration ($m\,s^{-2}$) |
| $k$ | fitting parameter in Eq. (2) |
| $L$ | location of three-phase contact line (mm) |
| $n$ | fitting parameter in Eq. (2) |
| $Q$ | volumetric flow rate ($ml\,h^{-1}$) |
| $W$ | width of microchannel (m) |
| MWF | minimum wetting flow rate per unit microchannel width ($ml\,h^{-1}\,mm^{-1}$) |

*Greek letters*

| | |
|---|---|
| $\alpha$ | aspect ratio |
| $\delta$ | thickness of liquid film (m) |
| $\gamma$ | angle between the tangent line of gas-liquid interface profile and the side wall (°) |
| $\mu$ | viscosity (Pa s) |
| $\theta$ | equivalent contact angle (°) |
| $\rho$ | density ($kg\,m^{-3}$) |
| $\sigma$ | surface tension ($N\,m^{-1}$) |
| $\Gamma_{min}$ | mass flow rate per wetted width ($kg\,s^{-1}\,m^{-1}$) |

imental data, where the influence of fluid physical properties and channel dimension is revealed to a large extent.

## 2. Experimental

### 2.1. Falling film microreactor design

Five single-channel falling film microreactors (denoted as SFFMR I–V, respectively) with different dimensions were milled on the substrate of polymethyl methacrylate (PMMA) using a precision machine (KPC-30a). The reactor configuration and their geometry dimension were shown in Fig. 1 and Table 2, respectively. The inlet of SFFMR was formed by sticking a transparent adhesive tape onto the plate (the shadow area shown in Fig. 1). Before each run, the microreactor was cleaned by ultrasonic method and then dried under clean environment.

### 2.2. Experimental setup

Fig. 2 shows the experimental setup. A syringe pump was used to drive the liquid into the microchannel, whereby a falling liquid film was generated. When the flow was stable, a high-speed CCD camera was used to observe the flow pattern in the microchannel. The background illumination was provided by a cold fiber optical lamp positioned on the backside of the reactor. First, a very low liquid flow rate was used and increased carefully until the presentence of complete falling film. Then, the flow rate was decreased gradually until the dry patches were present. During each experimental run,

**Table 2**
Dimension of SFFMRs.

| SFFMR | I | II | III | IV | IV |
|---|---|---|---|---|---|
| Depth (mm) | 0.3 | 0.3 | 0.3 | 0.5 | 1 |
| Width (mm) | 0.5 | 1 | 2 | 1 | 1 |
| Aspect ratio | 0.6 | 0.3 | 0.15 | 0.5 | 1 |
| Length (mm) | | | 60 | | |

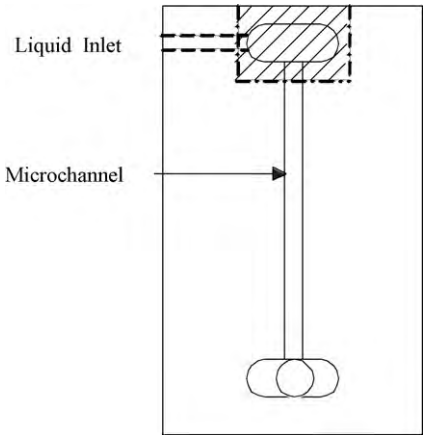


**Fig. 1.** Schematic configuration of singe-channel falling film microreactor.

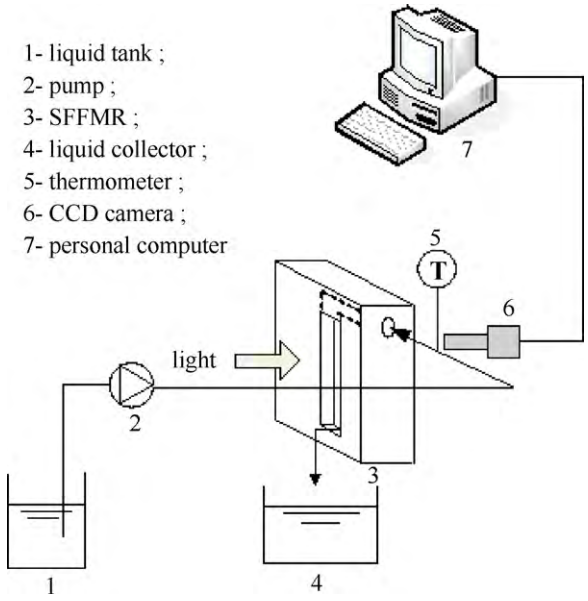


**Fig. 2.** Experimental setup with falling film microreactors.

**Table 1**
Minimum flow rate and film thickness correlations for traditional falling film reactors [5,10–13].

| Falling film type | Criteria | Correlations | Authors |
|---|---|---|---|
| Falling film along vertical surface | Force balance | $\Gamma_{min} = 1.69(\mu\rho/g)^{1/5}[\sigma(1-\cos\theta)]^{3/5}$<br>$\delta_{min} = 1.72[\sigma(1-\cos\theta)/\rho]^{1/5}(\mu/\rho g)^{2/5}$ | Hartley and Murgatroyd [10] |
| | Minimum total energy | $\Gamma_{min} = 0.803(\mu\rho/g)^{1/5}\sigma^{3/5}$<br>$\delta_{min} = 1.34[\sigma/\rho]^{1/5}(\mu/\rho g)^{2/5}$ | |
| | Empirical correlation | $\Gamma_{min} = (\mu\rho\sigma^3/g)^{1/5}[0.67(1-\cos\theta)^{0.623} + 0.26(1-\cos\theta)^{2.092}]$<br>$\delta_{min} = [15\mu^2\sigma/\rho^3 g^2]^{1/5}(1-\cos\theta)^{0.22}$ | El-Genk et al. [11] |
| | Minimum total energy | $\Gamma_{min} = 1.018(\mu\rho/g)^{1/5}[\sigma(1-\cos\theta)]^{3/5}$ | Doniec [12] |
| Falling film along vertical tube | Empirical correlation | $\Gamma_{min} = 0.13((1-\cos\theta)\sigma)^{0.764}\rho^{0.255}\mu^{-0.018}$ | Morison et al. [13] |
| | Experimental data | $\Gamma_{min} = 0.222$ (water as fluid) | Paramalingam et al. [5] |

**Table 3**
Physical properties of the liquids used in this study.

| Liquid | Static contact angle ($\theta$)[a] (°) | Receding contact angle ($\theta_R$)[a] (°) | Surface tension ($\sigma$) (mN m$^{-1}$) | Density ($\rho$) (kg m$^{-3}$) | Viscosity ($\mu$) (mPa s) |
|---|---|---|---|---|---|
| Deionized water | 79.7 | 49.8 | 72.08 | 0.996 | 0.92 |
| 12 wt% EG | 77.7 | 49.8 | 66.4 | 1.012 | 1.12 |
| 25 wt% EG | 70.3 | 45 | 61.06 | 1.03 | 1.77 |
| 50 wt% EG | 66.1 | 41 | 53.29 | 1.06 | 4.05 |
| 110 ppm SLS | 76.7 | 49.8 | 70.45 | 0.996 | 0.92 |
| 200 ppm SLS | 75.5 | 48.8 | 65.31 | 0.996 | 0.92 |

[a] Refers to that on the micromachined PMMA surface.

the critical flow rates were determined. To ensure the experimental accuracy, the liquid flow rate was reduced stepwise by as little as 0.2 ml h$^{-1}$. Here, the critical flow rate from 'complete falling film flow' to 'falling film flow with dry patches' (WDCF) was defined as the minimum wetting flow rate (MWF). In the present experiment, several liquids with different physical properties were used including deionized water, 12, 25 and 50 wt% ethylene glycol (EG), 110 and 200 ppm sodium laurylsulfate (SLS) aqueous solutions. For DWCF at lower concentration ($\leq$5.2 wt%) of ethylene glycol (EG), the experimental error was somewhat large. But the smallest value among three repeated data was even seven times higher than SDCF. For higher concentration of EG, the experimental error was less than 33%. Experimental error in WDCF was less than 8%.

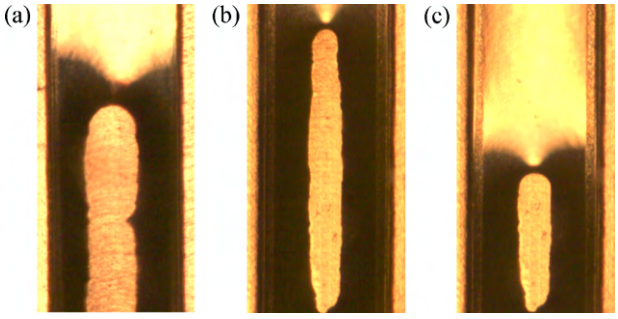


**Fig. 4.** Wetting process in SFFMR II with deionized water as fluid: (a) the top part of dry strip, $Q$ = 9 ml h$^{-1}$; (b) dry patches, $Q$ = 54 ml h$^{-1}$; (c) dry patches, $Q$ = 97.2 ml h$^{-1}$.

### 2.3. Contact angle measurement

Wettability denotes the ability of a liquid to spread on a surface and can be represented by contact angle. Contact angle is related with not only the physical properties of liquid and solid, but also the cleaning degree, roughness and the formation way of solid surface. In the present work, the microchannel surface of falling film microreactors was fabricated on PMMA by a micromilling machine. In order to obtain the contact angle data on this surface, it was first cleaned by ultrasonic method, then dried under clean environment. Both static and dynamic receding contact angles of several solutions on the microchannel surface were measured with an optical contact angle measuring device (OCA15EC, Dataphysics, Germany). Meanwhile, the surface tension of the investigated solutions was also determined with this equipment. All these measurements were performed at room temperature (~25 °C). The results of measurement were listed in Table 3, along with the relevant data of viscosity and density of solutions cited from the open literature [14].

## 3. Results and discussion

### 3.1. Flow pattern and wetting behavior in microchannels

Flow patterns observed in the microchannel of SFFMRs were similar to those we have observed previously in multi-channel falling film microreactors [8]. They were identified as 'corner rivulet flow', 'falling film flow with dry patches' and 'complete falling film flow', as shown in Fig. 3. For 'corner rivulet flow', liquid flows as two wedges in the corners with dry strip in the middle of the microchannel, and the length of the dry strip is almost the same as the microchannel. As the second flow pattern occurs, the dry strip was partly wetted by the liquid film and formed dry patches. The third one displays as a complete falling film with the interface profile taking a form of flowing meniscus due to the capillary effect [15].

Upon increasing the flow rate in the flow pattern of falling film with dry patches, the microchannel began to be mainly wetted by almost the same way as that seen in traditional falling film reactors. This way was that the liquid film on the top of the dry strip or patch became thicker and thicker with increasing flow rate, causing the liquid to wet the top part of the dry strip or patches (Fig. 4). In detail, at a certain flow rate, there existed a spot above dry area determined by the balance between hydrodynamic force and surface tension. When the flow rate was increased, the hydrodynamic energy of liquid tended to be higher so that this balance was broken. Then the liquid began to wet the wall and a new balance was established [16]. This way could be observed throughout the wetting process of the microchannel for all the solutions. However, it was also found that a part of dry strip was wetted by the liquid

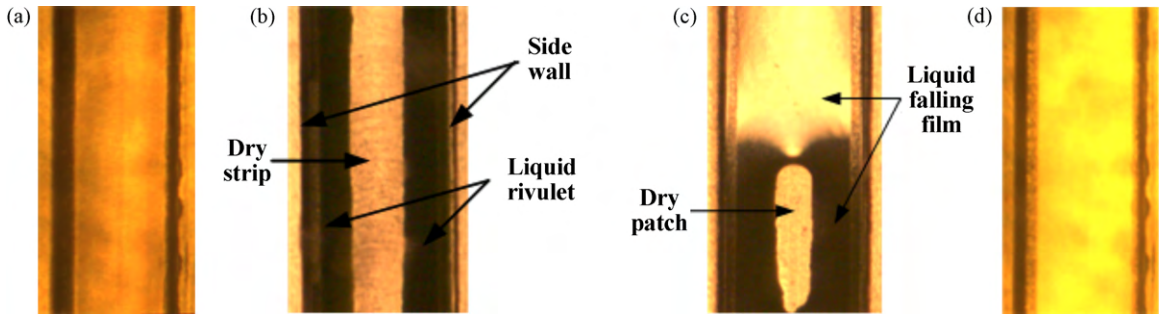


**Fig. 3.** Flow patterns with deionized water as fluid in SFFMR II: (a) microchannel without liquid; (b) corner rivulet flow, $Q$ = 4.8 ml h$^{-1}$; (c) falling film flow with dry patches, $Q$ = 97.2 ml h$^{-1}$; (d) complete falling film, $Q$ = 180 ml h$^{-1}$.

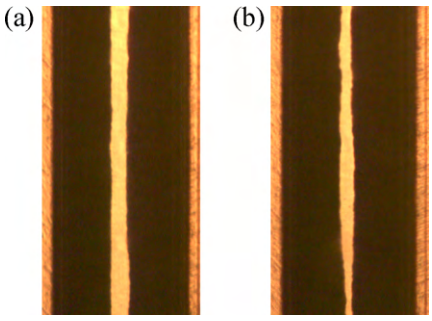


**Fig. 5.** Wetting process of dry stripes in SFFMR II with 12 wt% EG solution as fluid: (a) $Q = 7.2\ ml\ h^{-1}$; (b) $Q = 9\ ml\ h^{-1}$.

film from its two sides, which made the dry strip narrower and narrower with increasing flow rate until this part of dry strip was wetted (Fig. 5a and b). This way of wetting was only observed during the transition from 'corner rivulet flow' to the 'falling film flow with dry patches' for solutions of ethylene glycol. This might be a result of the decrease of contact angle and surface tension with these solutions (see Table 3). For EG solutions with higher concentration, the lower surface tension indicated that a much smaller hydrodynamics force is needed for the build up of a new balance. Therefore the dry patch tends to be wetted easier from its both sides when the flow rate is increased.

### 3.2. Critical flow rate

For liquid film in traditional falling film reactors, there exists a critical flow rate above which the liquid can wet the solid surface completely. Otherwise, dry patches may be present [17]. For falling film in microchannels, the critical flow rate may exist between three flow patterns as described above. That is, the critical flow rates from 'corner rivulet flow' to 'falling film flow with dry patches' (designated as dry strip to dry patches critical flow rate, SDCF),from 'falling film flow with dry patches' to 'complete falling film flow' (designated as dry to wetted critical flow rate, DWCF), and from 'complete falling film flow' to 'falling film flow with dry patches' (designated as wetted to dry critical flow rate, WDCF). During experiments, all relevant flow rate data have been measured three times. Fig. 6 shows the average critical flow rate measured between each flow pattern observed for EG solution with different concentrations in SFFMR II. It was found that DWCF was about 8–14 times higher than WDCF. As the flow rate was increased to determine DWCF, the advanced angle was involved whereas the receding angle was found as the flow rate was decreased to obtain WDCF. This contact angle hysteresis was mainly caused by such factors as roughness of PMMA surface [18], surface heterogeneity [19] and liquid penetration and surface swelling [20]. As a consequence, a large difference between DWCF and WDCF was observed, which is also much larger than that observed in traditional falling film reactors [21]. This could be explained by the fact that the surface tension is dominant in the microchannel and a much higher resistance of liquid wetting from three solid walls should be present therein comparing to one solid wall case in traditional falling film reactor [16]. Thus in the microchannel the surface tension force can afford comparatively high hydrodynamic and static pressures. It is further shown in Fig. 6 that all critical flow rates decreased with an increase in EG concentration, which might be a result of the decrease in contact angle and surface tension of solutions. From the above discussion, it can be concluded that the pre-wetting of the microchannel, lower contact angle and surface tension are three major factors necessary to form complete falling film at sufficiently low liquid flow rate. For ease of comparison with traditional falling film correlations, a minimum wetting flow rate (MWF) was defined here for falling film microreactors as WDCF per unit width of microchannel.

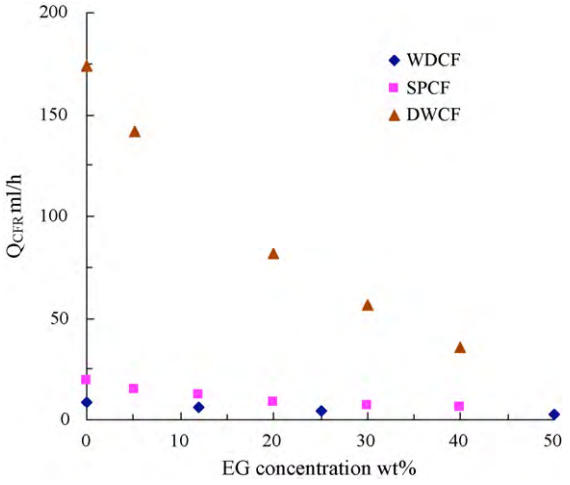


**Fig. 6.** The critical flow rate (CFR) between different flow patterns as a function of EG concentration in SFFMR II.

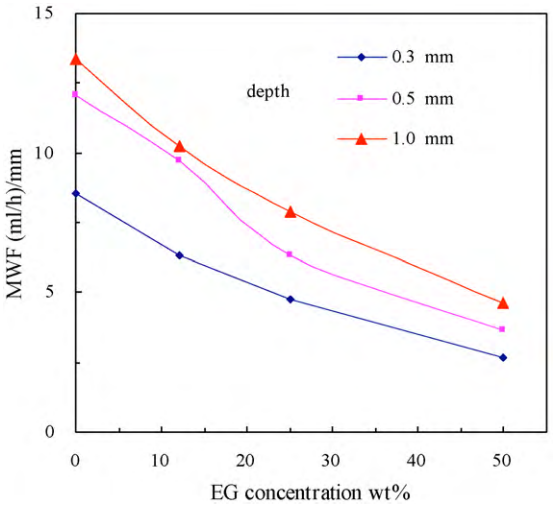


**Fig. 7.** Effect of microchannel depth on MWF (width of 1 mm).

### 3.3. Effect of microchannel geometry on MWF

The presence of 'complete falling film' flow pattern contributes substantially to mass transfer and reaction process. The minimum wetting flow rate is thus necessary to be determined in order to ensure the presence of this favorite flow pattern inside microchannels. MWF for traditional falling film depends on the properties of fluid and solid surface. Due to the combination of capillary forces and micron-sized channel geometry, the gas–liquid interface inside microchannels was observed to be meniscus instead of being flat [15]. The thinnest part of liquid film was located in the middle of microchannel bottom. Therefore, for falling film in microchannels, channel geometry also plays an important role.

Fig. 7 shows the variation of MWF with the depth of microchannel observed in this study. It can be seen that MWF increases upon increasing the depth of microchannel. Thus it implies that increasing the depth of microchannel does not help keep the falling liquid film complete at lower liquid flow rate. This could be explained by the following discussion. We have obtained the relationship between the film thickness in the middle of channel bottom, con-

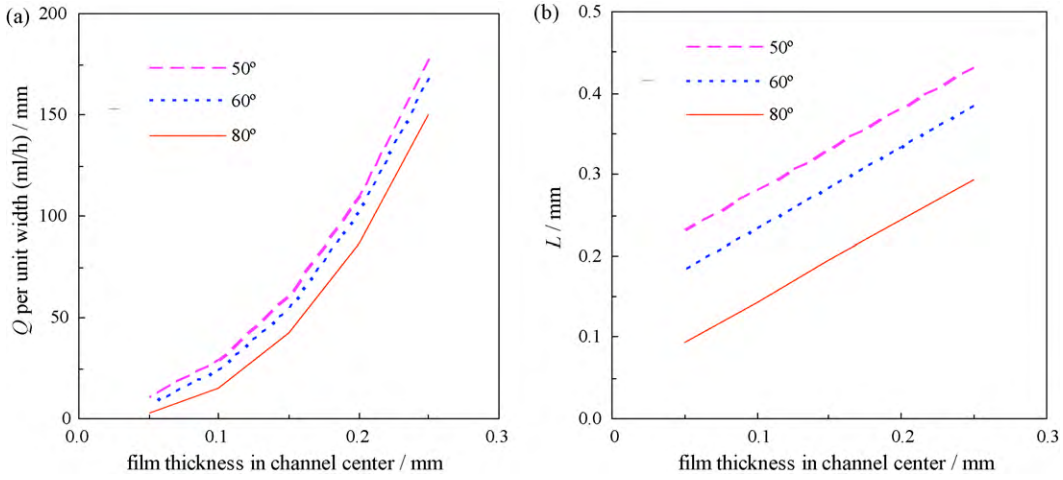


**Fig. 8.** Variation of liquid flow rate (a) and the location of three-phase contact line (L) (b) with the thinnest liquid film thickness (deionized water; microchannel width of 1 mm).

tact angle and three-phase contact line via CFD stimulations using COMSOL PHYSICS 3.4. The simulations were performed under the presumption that the gas–liquid interface profile was a circular arc. A contact angle and the film thickness in the center of microchannel were firstly fixed. Then, the location of the three-phase contact line could be obtained by the following equation

$$L = \delta + \frac{W}{2\cos\ \theta}(1 - \sin\theta) \quad (1)$$

After the cross-sectional geometry of falling film was determined, a 2-dimension N–S equation was solved numerically by COMSOL PHYSICS 3.4. Then, an integration of the velocity profile in the simulation domain was performed to obtain the flow rate. The results of simulation are shown in Fig. 8. Fig. 9 further depicts two ways of movement of gas-liquid interface profile in deep and shallow microchannels as the liquid flow rate is decreased. For a deep one, the three-phase contact line located somewhere on the side wall of channel, namely, $\gamma$ (the angle between the tangent line of gas–liquid interface profile and the side wall) was equal to the contact angle $\theta$. Thus, as the liquid flow rate was decreased, the interface profile together with the three-phase contact line moved to the microchannel bottom. But for a shallow microchannel, the gas–liquid–solid three-phase contact line could locate right on the top of the side wall when the liquid flow rate was comparatively high, which caused $\gamma$ to be larger than $\theta$ (Fig. 9) [15,22]. As the liquid flow rate was decreased, the force balance on the liquid film could be maintained by deforming the interface profile towards the bottom of microchannel while still keeping the three contact line locate on the top of the side wall. Only after the flow rate was deceased to an extent that $\gamma$ was equal to $\theta$, would the three-phase contact line further move down in the same way as in deep one. The results in Fig. 8 have made it clear that the film in the channel center is thicker at the same flow rate when $\theta$ is comparatively large, which made the liquid film not easy to break up and that the three-phase contact line was much lower. Since in a shallow microchannel, the location of the three-phase contact line on the top of the side wall can make $\gamma$ bigger than the contact angle (Fig. 9a), a thicker liquid film was obtained at the same flow rate. Thus it is easy to understand that liquid film in the shallow microchannel tends to break up at somewhat lower flow rate than that observed in the deep one. As a conclusion, it is clear that decreasing microchannel depth contributes to keep the liquid film complete at relatively low flow rate.

The width of microchannel is another important factor in determining MWF. The variation of MWF as a function of microchannel width is shown in Fig. 10, where it appears that MWF increased significantly with the width of microchannel. For example, MWF for deionized water case (EG concentration at 0 wt%) increased from 1.87 to 19.83(ml $h^{-1}$)/mm when the microchannel width was increased from 0.5 to 2 mm. This can be clarified by the CFD calculations shown in Fig. 11. At the same liquid film thickness in the center of microchannel, the location of three-phase contact line on the side wall of wider microchannel was higher (Fig. 11a), which made the liquid flow rate per unit channel width relatively larger

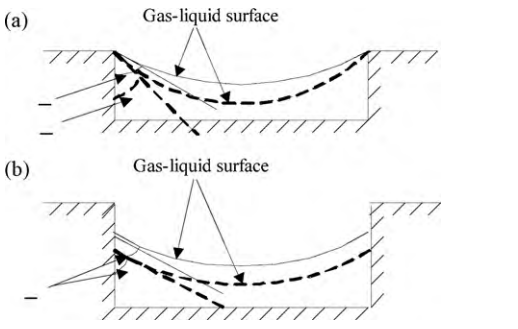


**Fig. 9.** Two ways of interface profile variation in shallow (a) and deep (b) microchannels.

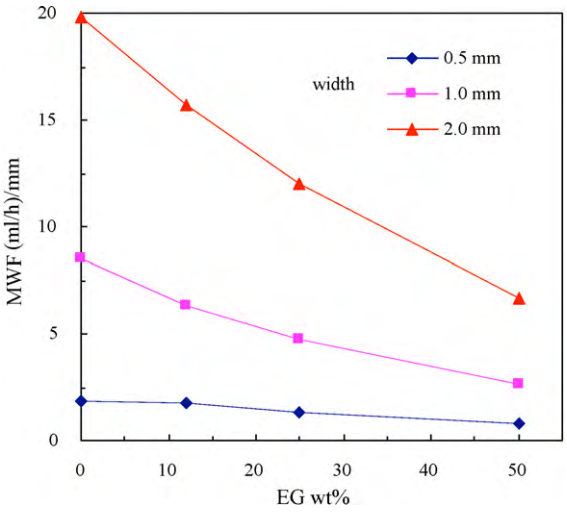


**Fig. 10.** Effect of microchannel width on MWF (depth of 0.3 mm).

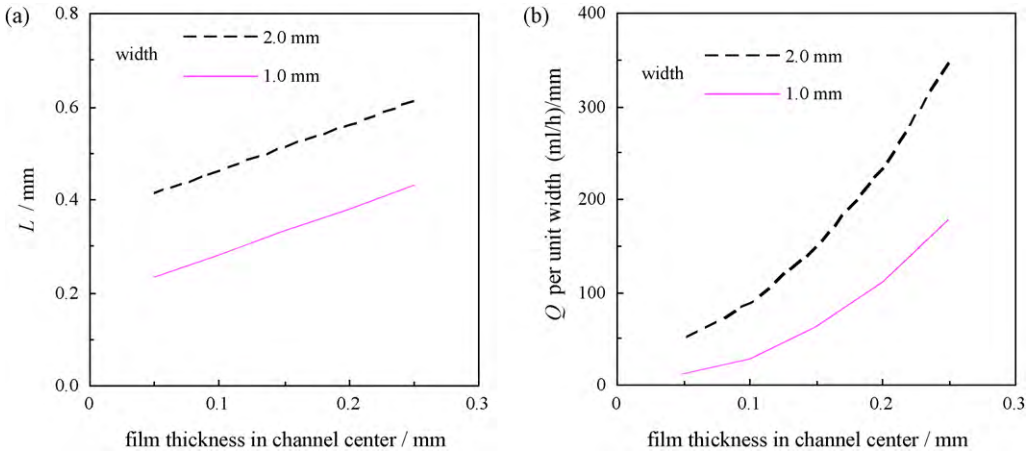


**Fig. 11.** Variation of three-phase contact line (a) and liquid flow rate per unit width (b) with liquid film thickness in the microchannel center (deionized water as fluid).

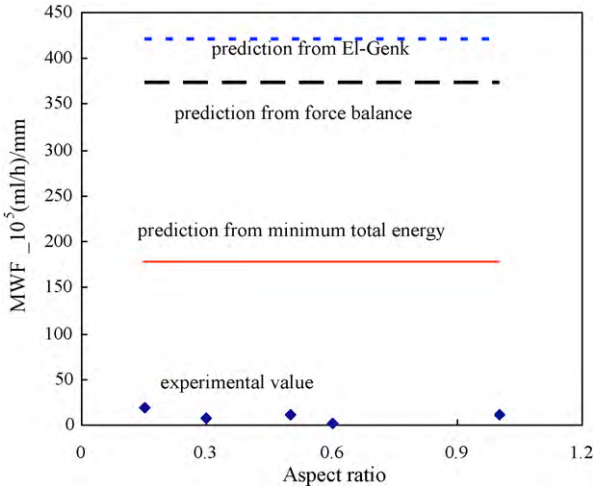


**Fig. 12.** Comparison of MWF between experimental data and predictions of the existing correlations (deionized water as fluid).

(Fig. 11b). Thus, in the wider microchannel, higher liquid flow rate is required to keep the liquid film complete. In other words, decreasing the width of microchannel can contribute to obtain complete falling film at relatively low flow rate.

### 3.4. Correlations to predict MWF

Fig. 12 compares the measured MWF of water in the current falling film microreactors to the prediction of the existing correlations proposed for traditional falling film reactors, where a considerable disagreement was found. Such kind of disagreement was also found for other fluids used in this study. For traditional falling film, the MWF was only dependent on the properties of fluid and solid surface. Nevertheless, for falling film in microchannels, the microchannel geometry turned to be another important factor as highlighted by our discussion in the above section. Table 4 further lists the minimum thickness of deionized water in traditional falling film reactors based on the equations shown in Table 1. It can be seen that the magnitude of liquid film thickness in traditional falling film reactors should be much larger than that in our microchannels, implying the inapplicability of the existing correlations. Therefore, a new correlation was proposed for the present falling film microreactors by using dimensionless analysis. That is,

$$\frac{MWF}{10^3 \times 3600} = k\frac{\mu}{\rho}\left(\frac{\rho(\sigma(1-\cos\theta))^3}{\mu^4 g}\right)^n \quad (2)$$

where $k$ and $n$ are the fitting parameters. As MWF (the critical flow rate from 'complete falling film flow' to 'falling film flow with dry patches') was measured via decreasing the flow rate gradually, the receding contact angle was used here for correlating. Based on the measured MWF data for different solutions (deionized water, 110–200 ppm SLS, 12–50 wt% EG solutions), the values of $k$ and $n$ can be obtained by the least square method, as shown in Table 5. It was first found that for all microchannels, a constant value of about 0.3 can be assumed for the parameter $n$ whereas $k$ varies with the microchannel aspect ratio. As we discussed before, decreasing either the width or depth of microchannel can lower MWF. Thus the influence of aspect ratio on MWF seems to be somewhat complicated and a fixed value could not be found for parameter $k$. Eq. (2) also suggests that the effect of surface tension and contact angle is more significant in microchannels, as reflected by the higher

**Table 5**
Fitting parameter in the proposed correlation to predict MWF in microchannels.

| Microchannel width (mm) × depth (mm) | Aspect ratio ($\alpha$) | $k \times 10^3$ | $n$ |
|---|---|---|---|
| 0.5 × 0.3 | 0.6 | 0.82 | |
| 1.0 × 0.3 | 0.3 | 3.7 | |
| 2.0 × 0.3 | 0.15 | 9.1 | 0.3 |
| 1.0 × 0.5 | 0.5 | 5.0 | |
| 1.0 × 1.0 | 1 | 5.4 | |

**Table 4**
Minimum thickness of traditional falling film.

| Liquid | Receding angle (°) | Minimum falling film thickness (mm) | | |
|---|---|---|---|---|
| | | Force balance | Minimum total energy | El-Genk' equation |
| Deionized water | 49.8 | 0.32 | 0.31 | 0.31 |
| 25 wt% EG | 45 | 0.38 | 0.38 | 0.31 |
| 50 wt% EG | 41 | 0.49 | 0.51 | 0.31 |
| 110 ppm SLS | 49.8 | 0.32 | 0.31 | 0.37 |
| 200 ppm SLS | 48.8 | 0.31 | 0.30 | 0.48 |

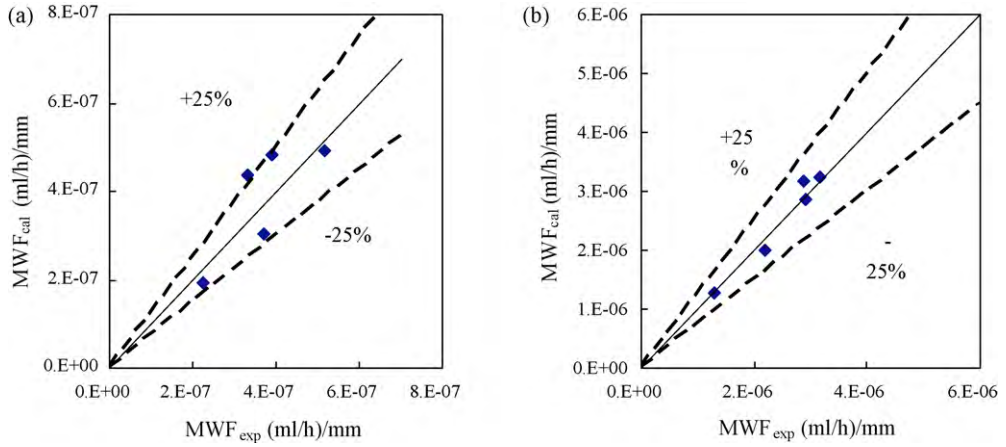


**Fig. 13.** Comparison between measured MWF per unit microchannel width and prediction of Eq. (2): (a) SFFMR I, $k = 0.00082$; (b) SFFMR V, $k = 0.0054$.

power exponent associated with $\sigma(1 - \cos\theta)$ than that found in traditional correlations (0.9 instead of 3/5). Fig. 13 further depicts the measured MWF in two microchannels and its comparison with the prediction of Eq. (2), where it can be seen that the proposed correlation here is sufficient to describe the present experimental data fairly well.

## 4. Conclusions

This paper reports an experimental investigation of flow pattern and liquid film break-up in single-channel falling film microreactors by using different fluids including deionized water, 110 ppm SLS, 200 ppm SLS, 12–50 wt% EG.

Three flow patterns were observed as 'corner rivulet flow', 'falling film with dry patches', and 'complete falling film flow'. The transition flow rate between each flow pattern was determined, where it was found that DWCF was about 8–14 times higher than WDCF due to the hysteresis of contact angle. The critical flow rate was further observed to decrease with the surface tension and contact angle for concentrated EG solution. Two ways of channel wetting were also found upon increasing the flow rate in the flow pattern of falling film with dry patches.

To ensure the operation of microreactor under the favorite flow pattern of complete falling film flow, the minimum wetting flow rate (MWF) was measured in microchannels with different geometry. It was found that MWF increased with an increase in the microchannel width or depth. Due to the inapplicability of the existing correlations to predict MWF in the current falling film microreactors, an empirical correlation has been proposed based on the measured data, where the influence of fluid physical properties and channel dimension is revealed.

## Acknowledgements

This work has been supported financially by National Natural Science Foundation of China (nos. 20676129 and 20911130358), the Ministry of Science and Technology of China (no. 2009CB219903), Fund of Dalian Institute of Chemical Physics, CAS (no. K2009D01).

## References

[1] K. Jahnisch, M. Baerns, V. Hessel, W. Ehrfeld, V. Haverkamp, H. Lowe, C. Wille, A. Guber, Direct fluorination of toluene using elemental fluorine in gas/liquid microreactors, J. Fluorine Chem. 105 (2000) 117–118.
[2] K.K. Yeong, A. Gavriilidis, R. Zapf, V. Hessel, Experimental studies of nitrobenzene hydrogenation in a microstructured falling film reactor, Chem. Eng. Sci. 59 (2004) 3491–3494.
[3] H. Ehrich, D. Linke, K. Morgenschweis, M. Baerns, K. Jahnisch, Application of microstructured reactor technology for the photochemical chlorination of alkylaromatics, Chimia 56 (2002) 647–653.
[4] N. Steinfeldt, R. Abdallah, U. Dingerdissen, K. Jahnisch, Ozonolysis of acetic acid 1-vinyl-hexyl ester in a falling film microreactor, Org. Process Res. Dev. 11 (2007) 1025–1031.
[5] S. Paramalingam, J. Winchester, C. Marsh, On the fouling of falling film evaporators due to film break-up, Food Bioprod. Process. 78 (2000) 79–84.
[6] K.J. Kim, N.S. Berman, B.D. Wood, The interfacial turbulence in falling film absorption: effects of additives, Int. J. Refrig. 19 (1996) 322–330.
[7] G. Karimi, M. Kawaji, Flow characteristics and circulatory motion in wavy falling films with and without counter-current gas flow, Int. J. Multiphase Flow 25 (1999) 1305–1319.
[8] H.C. Zhang, G.W. Chen, J. Yue, Q. Yuan, Hydrodynamics and mass transfer of gas-liquid flow in a failing film microreactor, AIChE J. 55 (2009) 1110–1120.
[9] A. Oron, S.H. Davis, S.G. Bankoff, Long-scale evolution of thin liquid films, Rev. Mod. Phys. 69 (1997) 931–980.
[10] D.E. Hartley, W. Murgatroyd, Criteria for the break-up of thin liquid layers flowing isothermally over solid surfaces, Int. J. Heat Mass Transfer 7 (1964) 1003–1015.
[11] M.S. El-Genk, H.H. Saber, Minimum thickness of a flowing down liquid film on a vertical surface, Int. J. Heat Mass Transfer 44 (2001) 2809–2825.
[12] A. Doniec, Flow of a laminar liquid film down a vertical surface, Chem. Eng. Sci. 43 (1988) 847–854.
[13] K.R. Morison, Q.A.G. Worth, N.P. O'Dea, Minimum wetting and distribution rates in falling film evaporators, Food Bioprod. Process. 84 (2006) 302–310.
[14] M.H. Oyevaar, R.W.J. Morssinkhof, K.R. Westerterp, Density, viscosity, solubility, and diffusivity of carbon dioxide and nitrous oxide in solutions of diethanolamine in aqueous ethylene glycol at 298 K, J. Chem. Eng. Data 34 (1989) 77–82.
[15] K.K Yeong, A. Gavriilidis, R. Zapf, H.J. Kost, V. Hessel, A. Boyde, Characterisation of liquid film in a microstructured falling film reactor using laser scanning confocal microscopy, Exp. Therm. Fluid Sci. 30 (2006) 463–472.
[16] X. Wang, X. Peng, J. Min, T. Liu, Hysteresis of contact angle at liquid solid interface, J. Eng. Thermophys. 23 (2002) 67–68.
[17] Y. Sutjiadi-Sia, R. Eggers, Lateral wetting angle of falling film in dense fluid, Int. J. Heat Mass Tranfer 51 (2008) 3608–3614.
[18] M. Shoji, X.Y. Zhang, Study of contact-angle hysteresis – (in relation to boiling surface wettability), JSME Int. J. B-Fluid T 37 (1994) 560–567.
[19] L.W. Schwartz, S. Garoff, Contact-angle hysteresis on heterogeneous surfaces, Langmuir 1 (1985) 219.
[20] R.V. Sedev, J.G. Petrov, A.W. Neumann, Effect of swelling of a polymer surface on advancing and receding contact angles, J. Colloid Interface Sci. 180 (1996) 36–42.
[21] D.M. Maron, G. Ingel, N. Brauner, Wettability and break-up of thin-films on inclined surfaces with continuous and intermittent feed, Desalination 42 (1982) 87–96.
[22] R. Seemann, M. Brinkmann, E.J. Kramer, F.F. Lange, R. Lipowsky, Wetting morphologies at microstructured surfaces, Proc. Natl. Acad. Sci. U.S.A. 102 (2005) 1848–1852.